Nuclear Materials and Energy 000 (2016) 1–7

Contents lists available at ScienceDirect

Nuclear Materials and Energy

journal homepage: www.elsevier.com/locate/nme

Precipitation of carbides in F82H steels and its impact on mechanical strength

S. Kano[a,*], H.L. Yang[a], R. Suzue[b], Y. Matsukawa[a], Y. Satoh[a], H. Sakasegawa[c], H. Tanigawa[c], H. Abe[d]

[a] Institute for Materials Research, Tohoku University, 2-1-1 Katahira, Aoba, Sendai, Miyagi 980-8577, Japan
[b] Graduate School of Engineering, Tohoku University, 6-6-04, Aramaki, Aoba, Sendai, Miyagi 980-8579, Japan
[c] Fusion Research and Development Directorate, Japan Atomic Energy Agency, 2-166 Omotedate, Obuchi, Rokkasho, Aomori 039-3212, Japan
[d] Nuclear Professional School, School of Engineering, The University of Tokyo, 2-22, Shirakata-Shirane, Tokai-mura, Ibaraki 319-1188, Japan

ARTICLE INFO

Article history:
Available online xxx

Keywords:
F82H steel
Carbide
TEM
Extracted residue test (ERT)
Precipitation strengthening

ABSTRACT

The precipitation of carbides in F82H steel and its model steel (Fe-0.2TaC) were investigated by transmission electron microscopy (TEM) and extracted residue tests (ERT). The effects of tempering on the precipitation in F82H steels were elucidated on the basis of the characterization of carbides, as well as the quantitative estimation of precipitation strengthening at room temperature. Firstly, the number density of precipitates was measured by extracted residue test in Fe-0.2TaC and tempered F82H steel, and compared with the TEM observation. It was found that the ratio of volume fraction between the TEM and the ERT was respectively 1.84 and 0.54 for Fe-0.2TaC and tempered F82H steel, revealing that the collection probability of ERT strongly depends on the precipitate features, size and number density. Effects of annealing on the precipitation in F82H steels were investigated by ERT. The amount of carbide showed a non-linear relationship to tempering parameter, $TP = T(20 + \log t)$. It steeply increased in the TP range from 15.3 to 16.2. The precipitation strengthening in F82H steel was estimated to be about 5–10% relative to its proof strength, suggesting that the carbides in F82H steel have a minor role on the tensile strength at room temperature, though these precipitates are greatly beneficial for improving the creep and radiation resistance at elevated temperatures.

1. Introduction

Among the various reduced activation ferritic/martensitic steels (RAFMs), F82H (Fe-8Cr-2W-V-Ta) steels have been considered as one of the promising candidate materials for the Japanese test blanket module (TBM) system in ITER, because of their excellent heat resistance and good irradiation resistance [1,2]. The satisfactory mechanical performance of this material in terms of strength, creep and toughness, is due to their unique microstructure. The microstructural of F82H steel is described as tempered ferritic/martensitic structure composed of lath martensite and precipitates such as $M_{23}C_6$ (M = Cr, W and Fe) and MX (M = Ta, V; X = C, N). These carbides are apparently of great importance to influence the mechanical properties, therefore, many studies on the precipitates in F82H steel have been investigated [3–7].

On the other hand, it is easy to notice that the characterizations of the carbides, including particle size, number density, chemical composition and so on, were carried out via transmission electron microscope (TEM) observations in most of the investigations [3,4]. Owing to the very high resolution and unique crystallographic structure determination ability, TEM is a very powerful tool to characterize the fine particles in a wide variety of materials. In terms of macro-scale characterizations, however, the shortage of view field and less efficiency are the weaknesses of TEMs. It is not suitable to measure coarse sized particles such as inclusions, which generally possess the size of several μm [5]. Further, TEM has difficulty in the quantitative estimation of precipitate and dislocation densities in F82H steels, because of the complicated and relatively large scale microstructure due to tempering and martensitic transformation [1]. This results in a large margin of error in the estimated data. Thus, TEM observation is insufficient to well build the microstructure database for F82H steel. A more precise estimation of carbide density is expected by macroscale experiments like extracted residue test (ERT) combined with other techniques.

* Corresponding author. Fax. +81-22-215-2066.
E-mail address: kano.sho0215@gmail.com (S. Kano).

http://dx.doi.org/10.1016/j.nme.2016.09.017

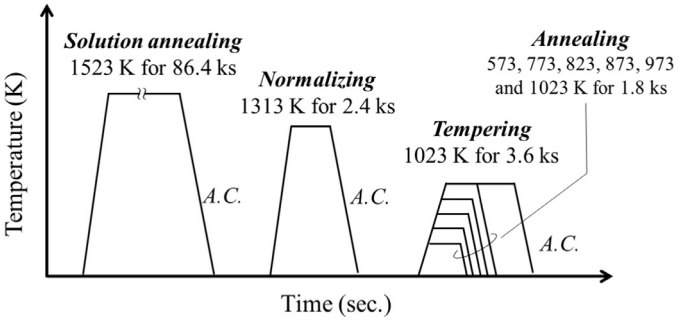

Fig. 1. Thermal history of F82H steels. A.C. denotes air cooling. Heating and cooling rates were 2 and 3 K/s, respectively.

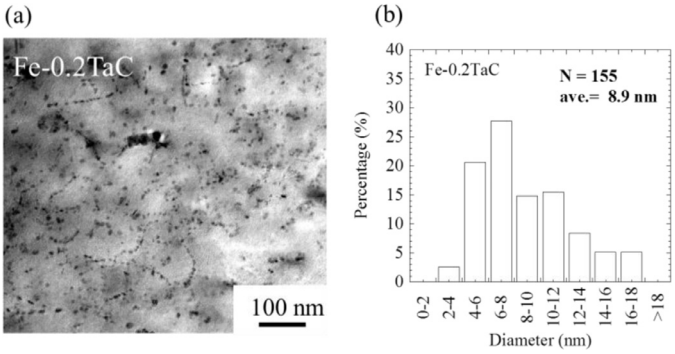

Fig. 2. (a) TEM bright field image of Fe-0.2TaC model alloy, and (b) the size distribution of TaC. N and ave. stand for the number of measurement and the averaged size.

Nagasaka et al. [6] proposed a combination of ERT, X-ray diffraction (XRD) and inductively coupled plasma (ICP) analyses to analyze the precipitation in the thermally aged F82H steels. Since the average sizes of MX and $M_{23}C_6$ in the steel were 60 and 118 nm [3,7], respectively, they were successful in filtering the carbides. However, they underestimated the amount of carbides, especially MX, which our range size is less than 50 nm [8–10]. The purpose of the present study is, therefore, to investigate the precipitation of carbides in F82H steels by TEM and ERT. The precipitation will be investigated tempered and annealed F82H steels and its model alloys to get insights into the corresponding precipitation strengthening.

2. Experimental procedure

Two kinds of experimental materials were used in the present study. One is F82H steel (Fe-0.098C-7.81Cr-1.88W-0.44Mn-0.19V-0.037Ta), and the other is the ternary model alloy (Fe-0.015C-0.19Ta), which will be called Fe-0.2TaC hereafter. The carbon concentration of F82H steel is slightly lower than that of the original F82H-IEA (0.1 wt.%C) [5]. In order to prevent carburizing and decarburizing, the specimens were acidized using a solution of 20% hydrochloric acid and balanced methanol for 43.2 ks. Then, the specimens were capsuled into clean quartz tubes with high purity argon gases. Thermal history of the three-step heat treatment of F82H steel is shown in Fig. 1. The specimens firstly underwent the solution annealing at 1523 K for 86.4 ks to homogenize the alloying elements. Subsequently the specimens were normalized at 1313 K for 2.4 ks. Afterwards, the specimens were tempered at 573, 773, 823, 873, 973 and 1023 K for 1.8 ks, or 1023 K for 3.6 ks, respectively. In all of the heat treatments, the heating and cooling rate were respectively set as 2 and 3 K/s, also, the occurrence of martensitic transformation in this cooling rate was confirmed from the thermal expansion measurement. For the F82H steels, the one tempered at 1023 K for 3.6 ks is named as tempered F82H, as this heating regime is the same with F82H-IEA tempering process; the rest of the specimens (annealed at 573, 773, 823, 873, 973 and 1023 K for 1.8 ks) are named as annealed F82H. For the Fe-0.2TaC, the specimens were tempered at 1123 K for 3.6 ks, after a solution annealing at 1523 K for 43.2 ks followed by water quenching.

The ERT was conducted using an AA solution, the mixture of 10% acetyl acetone, 10% tetra methyl ammonium chloride and balanced methanol, with keeping the electric current of roughly 100 mA at room temperature [6,7]. At this electric current, it was examined that the matrix could be electrochemically dissolved and precipitates were stably remained in the etchant solution [11,12]. The remained precipitates were collected on a membrane filter with 50 nm pore size by vacuum percolation. The extracted residues were, then, weighed using an electronic balance with an accuracy of ± 0.1 mg, which was roughly equivalent to 0.1% of the total weight of residue obtained in each test. Afterwards the XRD analysis was performed on the extracted residues on an X-ray diffractometer (Rigaku, Ultima IV) with a Cu target at 40 kV and 40 mA. The size and number density of carbides were also investigated by TEM, so as to compare to the results attained from ERT. Twin-jet electro-polishing to achieve electron transparent F82H specimens was carried out in a solution containing 8% perchloric acid and acetic acid at room temperature.

Table 1
Weight percentage of extracted residue in Fe-0.2TaC model alloy.

Test No.	Extracted residue, W (%)
1	0.242
2	0.234
3	0.251
AVE	0.242

3. Results and discussion

3.1. Comparison of particle volume fractions obtained by TEM observation and ERT

3.1.1. Fe-0.2TaC

Fig. 2 shows the bright field (BF) image of Fe-0.2TaC and the size distribution of carbides. It is noticed from the BF image (Fig. 2(a)) that numerous fine TaC particles were dispersed in the matrix, appearing in either spherical or thin foil shape, which is consistent to a previous study [13]. The thickness of the observed region was determined by the thickness fringe technique, and the number density of carbides was estimated as 7.9×10^{21} m^{-3}. As shown in Fig. 2(b), the unimodal size distribution was observed ranging from roughly 2 to 20 nm with a peak at around 6–8 nm. Also, average particle size, which is defined as the length of the major axis, was estimated as roughly 8.9 nm, which is consistent with our previous study [14]. Thereby, the volume fraction of TaC was calculated as 0.289%, assuming the particles were spherical.

The number density of TaC was also examined by the ERT. The results are listed in Table 1. Weight percentage of extracted residue, W, is calculated according to the following equation [11]:

$$W = \frac{W_{PPT}}{\Delta W} \times 100\% \quad (1)$$

where, W_{PPT} is the weight of precipitates and ΔW is the weight difference of specimen between before and after ERT. The ERT was repeated three times, and the average weight percentage of the extracted residue was 0.242%, corresponding to a volume fraction of TaC of 0.157%. The volume fraction is obtained by multiplying the weight fraction with the density ratio (D_{matrix}/D_{ppt}),

Table 2
Precipitate characterizations by TEM and ERT in tempered F82H steel.

	TEM			Extracted residue test		
	MX	$M_{23}C_6$	SUM	MX	$M_{23}C_6$	SUM
Weight percentage of extracted residue, W (%)	–	–	–	0.07	1.91	1.98
Average diameter (nm)	24	55	–	–	–	–
Number density ($\times 10^{18}$ m^{-3})	9.8	135.5	–	–	–	–
Volume fraction ($\times 10^{-4}$)	0.7	118	118.7	3.6	212.6	216.2

where $D_{matrix} = 7.87$ g/cm^3 [15] is the density of the matrix and $D_{ppt} = 14.48$ g/cm^3 [16] is the density of the precipitates. Compared to the TEM observation result, it is noticed that the volume fraction of TaC was underestimated by ERT. The ratio between the volume fractions measured respectively by TEM and ERT methods in Fe-0.2TaC (V^{TEM}/V^{ERT}) was estimated as 1.84, indicating that roughly ~46% of the TaC particles were not counted in ERT tests.

The ERT was conducted using membrane filters whose pore size was 50 nm in the present study. Carbides possessing a size smaller than the pore size might leak through the membrane filter. Therefore, it is necessary to compare the number density of TaC evaluated by ERT to the one by TEM, in order to assume the loss ratio and improve the data reliability. Assuming the shape of TaC in extracted residue is spherical, the precipitate number density evaluated by ERT, N_{PPT}, can be calculated from the following equation:

$$N_{PPT} = \frac{W_{PPT}}{\Delta W}\frac{D_{matrix}}{D_{PPT}V_{PPT}} \quad (2)$$

where, V_{PPT} is volume of a particle. Accordingly, the average number density of TaC is calculated as 3.58×10^{21} m^{-3}. It is found that the value evaluated from ERT is nearly half of that examined by TEM; i.e. 7.9×10^{21} m^{-3}.

As revealed above, the ERT underestimated the amount of precipitates in Fe-0.2TaC in comparison to the TEM observation, presumably due to some carbide leakage through the filter, as the average size of TaC is much smaller than the filter pore size. The particles with size less than 50 nm simply pass through the filter. Nevertheless, TaC particle residues were indeed collected in each test, despite the fact that the number density of the particles were underestimated. This means that particles less than 10 nm can to be filtered using the ERT, even if the pore size in the filter is 50 nm. The mechanism of this phenomenon still remains unclear, but it may be related to the clogging of the filter pores and the agglomeration of the fine carbide powders. The 11 nm average sized fine $Y_2Ti_2O_7$ particles in an ODS martensitic steel had also been reportedly collected by a filter with 100 nm pore size in ERT in a previous study [17].

3.1.2. Tempered F82H steel

Similar estimations were also conducted on the tempered F82H steel which is tempered at 1023 K for 3.6 ks. Fig. 3 shows the results of the TEM observation. The lath martensitic structure was clearly observed as shown in Fig. 3(a). Two types of precipitates with distinct specifications were observed. Some of the carbides as indicated by solid triangles, were found to be preferentially located on the lath grain boundaries. Such precipitates generally were relatively larger in size which was about 55 nm. By the selected area electron diffraction (SAED) analysis, as shown in Fig. 3(c), these precipitates were analyzed to have a fcc structure and a lattice parameter of 1.06 nm. They are thus identified as $M_{23}C_6$ type carbide. On the other hand, the other type of precipitates denoted by open triangle was only found within the lath grains. These precipitates were much smaller compared to $M_{23}C_6$. These fine intra-granular precipitates are believed to be MX type carbides; namely TaC as shown in Fig. 4. The size and number density of carbides were estimated based on TEM observations and summarized in Table 2.

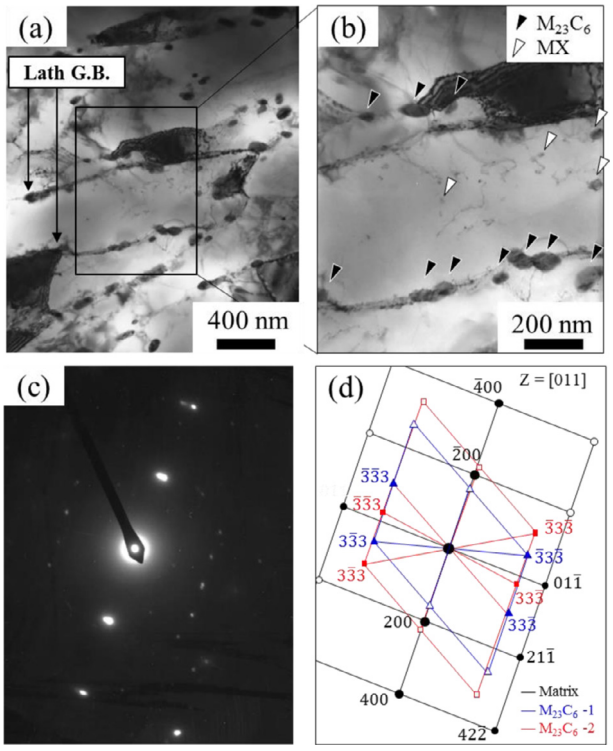

Fig. 3. TEM observation results of tempered F82H steel. (a) Low magnification of bright-field image. Lath grain boundary (G.B.) is indicated. (b) Magnified image from the inset rectangular in (a). Solid and open triangles indicate $M_{23}C_6$ and MX particle, respectively. (c) Selected area electron diffraction (SAED) pattern in (a). (d) The corresponding indices. Solid circles, triangles, squares denote diffractions from matrix, $M_{23}C_6$-1 and $M_{23}C_6$-2, respectively. Open symbols indicate background.

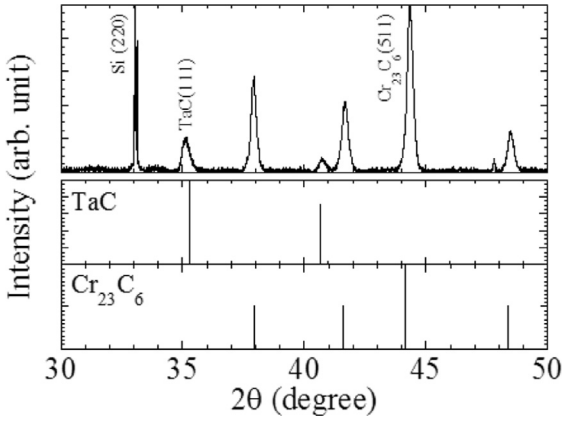

Fig. 4. XRD pattern of extracted residue from the tempered F82H steel. Si single crystal was used as reference. Standard diffractions of $Cr_{23}C_6$ (ICDD No. 01-089-2724) and TaC (ICDD No. 01-089-2724) were also shown.

As pointed out above, there are two types of carbides in F82H steel. In order to estimate the amounts of $M_{23}C_6$ ($Cr_{23}C_6$) and MX (TaC) quantitatively, XRD measurements were performed on the extracted residue. An example of the XRD pattern of extracted residue from tempered F82H is shown in Fig. 4. The most intense diffraction peaks in TaC (ICDD No. 01-089-2724) and $Cr_{23}C_6$ (ICDD No. 01-089-2724) are (111) and (511), respectively [18]. The intensity of diffracted peak shown in XRD pattern can be described by [19]:

$$I = F^2 N \frac{\rho}{\mu A} N_A \quad (3)$$

where F is the structure factor ($F_{MX} = 233.29$, $F_{MX} = 502.79$), N is the number of unit cell, μ/ρ is the mass absorption coefficient, A is the atomic number and N_A is the Avogadro constant. The dependence of X-ray scattering intensity on the Bragg angle is not taken into consideration in the present study, because the TaC (111) peak is quite close to $Cr_{23}C_6$ (511) peak. In general, the intensity of X-ray diffraction is determined by the number of unit cells and intensity derived from crystal structure. Although the crystal structure or space group of MX and $M_{23}C_6$ is the same: $Fm\bar{3}m$, the number of atoms need to form an unit cell is varied. These factors were consulted from the literature [20]. In the case of the μ/ρ, it depends on the weight ratio between MX and $M_{23}C_6$ in the extracted residue. However, the weight of MX was vanishingly small compared to the $M_{23}C_6$ as seen in Table 2. Hence, μ/ρ is approximately regarded as μ_{M23C6}/ρ_{M23C6}. Therefore, the weights of MX (W_{MX}) and $M_{23}C_6$ (W_{M23C6}) are calculated from the weight ratio (W_{MX}: W_{M23C6}), which is described as follows:

$$W_{MX} : W_{M23C6} = w_{MX} N_{MX} : w_{M23C6} N_{M23C6} = w_{MX} \frac{I_{MX}}{F_{MX}^2} : w_{M23C6} \frac{I_{M23C6}}{F_{M23C6}^2} \quad (4)$$

where w is the weight of a unit cell ($w_{MX} = 1.83 \times 10^{-21}$ g and $w_{M23C6} = 8.45 \times 10^{-21}$ g). Results of the extracted residue are summarized in Table 2. The weight percentage of extracted residue was 1.98%, agreeing well with a previous study [7]; the weight ratio of MX and $M_{23}C_6$ was estimated as 0.07:1.91. The volume fraction of precipitates (MX and $M_{23}C_6$) was then respectively calculated from the weight ratio; the density of $M_{23}C_6$ used is 7.07 g/cm^3 in $Cr_{23}C_6$ [21], and the density of F82H matrix used is 7.87 g/cm^3 [16]. The ratio between the precipitate volume fractions measured by TEM and ERT in tempered F82H (V^{TEM}/V^{ERT}) was evaluated as 0.54. It is worth noting that the ratio V^{TEM}/V^{ERT} in Fe-0.2TaC steel is distinctly different from that of F82H, indicating that the collection probability of carbides on the membrane filter is greatly influenced by the particle features, especially the size of particle. The size of TaC in Fe-0.2TaC model alloy is averaged as 8.9 nm, which is much smaller than the average size of MX (24 nm) and $M_{23}C_6$ (55 nm) in tempered F82H, thus the probability of the carbides passing through the filter is higher in fine carbide containing specimens.

It is also noted, in the case of F82H that the volume fraction of particles obtained by TEM (V^{TEM}) is less than that by ERT (V^{ERT}), which is opposite to what occurred in the Fe-0.2TaC model alloy, where $V^{TEM} > V^{ERT}$. This inconsistency is believed to originate from the particle features. The reason why $V^{TEM} > V^{ERT}$ in Fe-0.2TaC may be ascribed to the following two aspects: on the one hand, the size of TaC particles (averaged ~8.9 nm) is much smaller compared to the size of pores in the filter (50 nm), resulting in the high loss rate of particles in the ERT test; on the other hand, the microstructure of Fe-0.2TaC comprising of coarse grain and rare dislocations is fairly simple and clean (as revealed from Fig. 2(a)), making the TaC particles easily distinguishable from TEM micrographs. Thereby, the quantitative characterization of fine TaC particles by TEM observation is more reliable in comparison to ERT test in Fe-0.2TaC model alloy. On the contrary, the $V^{TEM} < V^{ERT}$ is found in F82H steel, which may also be explained by two reasons: firstly, the size of particles in F82H, either the averagely 24 nm-sized MX type carbides or the averagely 55 nm-sized $M_{23}C_6$ type carbides, are comparable or even larger than the pore size of the ERT employed filter, thus the vast majority of the precipitates is collected on the filters; secondly, the martensitic based microstructure in F82H is highly strained and possess high amounts of dislocations, which makes difficult to provide a clear particle-distinguishing image due to the overlapped contrast of dislocation cells and particles. What is more, F82H is not composed of coarse grains, but the messy and fine lath domains, along whose interfaces the $M_{23}C_6$ type carbides are precipitated (see Fig. 3). Thus, the full view of $M_{23}C_6$ particles is hardly possible be observed, involuntarily resulting in the under-estimated particle numbers in TEM micrograph. Consequently, the ERT test is a better approach to quantitatively characterize the precipitates in tempered F82H steel. In brief, it is the particles' specifications, such as the size and distribution, that greatly influence the method to quantitatively characterize them.

Table 3
ERT results on weight percentage of extracted residue of MX and $M_{23}C_6$ in annealed and tempered F82H steels exposed to various annealing.

Annealing conditions		Extracted residue (%)	
Temperature	$TP = T(20 + \log t)$	MX	$M_{23}C_6$
Normalized	5.46	< 0.01	0.13
573 K	11.29	< 0.01	0.07
773 K	15.23	< 0.01	0.15
823 K	16.21	0.09	1.85
873 K	17.39	0.10	1.97
1023 K	20.15	0.01	2.17
Tempered	20.46	0.07	1.91

3.2. Effects of tempering on precipitation in F82H steel

As revealed from the comparison results above, ERT is regarded as an appropriate way to quantitatively analyze the precipitates in F82H, where the microstructure of matrix is complicated and the size of particles is comparable to the pore size of filter. Therefore, the effects of tempering on the precipitation in F82H steel were evaluated by ERT, with the combined application of XRD analysis. The weights of MX and $M_{23}C_6$ for F82H steels annealed at various temperatures and their proportions were calculated and summarized in Table 3. The tempering parameter (TP), which is a commonly used factor to show the integrated effect of both temperature and holding time in tempered steels, is defined by the following equation [22]:

$$TP = T\,(20 + \log t) \quad (5)$$

where T is temperature in Kelvin and t is the holding time in hours. The TP for the tempered F82H steels was also summarized in Table 3.

Fig. 5 shows the weight percentage of extracted residue in annealed and tempered F82H steels as a function of TP. The open squares present the weight of extracted residue. The error bars indicate the standard deviations derived from three measurements of ERT for each specimen. Fig. 5 shows that the weight percentage of extracted residue was estimated as 0.2% when TP is lower than 15. Then the steep increase up to 1.8% was observed at the TP ranging from 15.3 to 16.2. Finally, it saturated at around 2.0% when TP is higher than 18. This indicates that the precipitation is very sensitive to the value of TP, which is presumably ascribed to the occurrence of a nucleation barrier for fine particles, especially for $M_{23}C_6$ in F82H steel at TP ranged between 15.2 and 16.2 [23]. Furthermore, it was found that the weight ratio between MX and $M_{23}C_6$ ($W_{ER,\,MX}/W_{ER,\,M23C6}$) decreased with the increase in TP. This

Please cite this article as: S. Kano et al., Precipitation of carbides in F82H steels and its impact on mechanical strength, Nuclear Materials and Energy (2016), http://dx.doi.org/10.1016/j.nme.2016.09.017

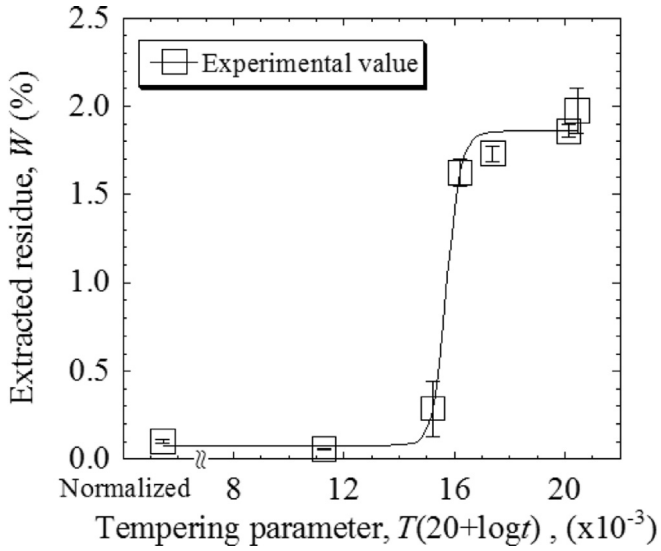

Fig. 5. Weight percentage of extracted residues in F82H steels as a function of tempering parameter. Error bars indicate the standard deviations.

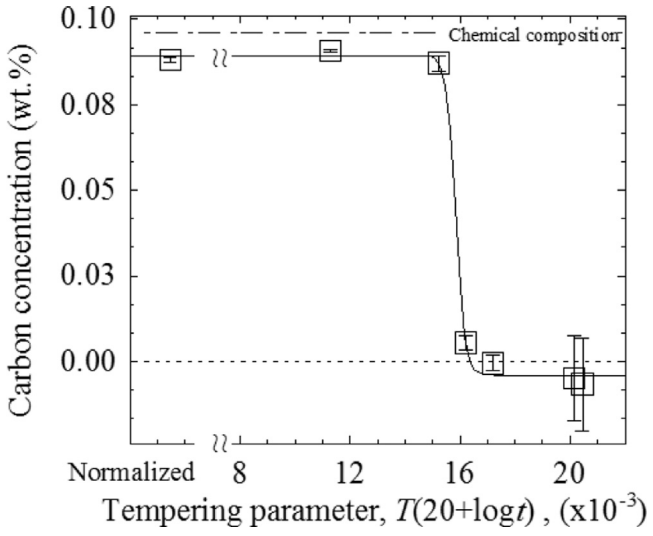

Fig. 6. Evaluation of dissolved carbon concentration in F82H matrix. The error bars indicate the standard deviation.

result can be explained by the formation energy of the carbide; the binding energy of chromium with carbon is much lower than tantalum [24]. Therefore, precipitation of $M_{23}C_6$ is presumed to proceed more easily during tempering compared to MX.

It needs to mention here that the experimental data measured via ERT are believed to be reliable at the annealing range from 823 to 1023 K. As seen from Table 3, sufficient amounts of particles were precipitated by high temperature annealing, the features of these particles were considered to be similar to the particles in tempered F82H steel. Nevertheless, the reliability of the data for Normalized, 573- and 773 K annealed specimens is not guaranteed. As revealed from Table 3, much less amount of particles was extracted in these specimens compared to the tempered one, suggesting that the precipitation process occurring in these specimens was still in an early stage. Thereby the particles probably possess a relatively smaller size, which may result in a greater loss ratio in the ERT test. However, even if the weight percentage of particles in Normalized, 573- and 773 K annealed specimens is underestimated, it is possible to speculate the actual value as per the loss ratio measured in Fe-0.2TaC model alloy. For example, to an upper bound, the actual precipitate weight fraction may be close to the value observed by TEM, i.e., nearly 2 times that measured by ERT test. Due to the significantly lower amount of precipitates in lower temperature annealed specimens (Normalized, 573- and 773 K), doubling the ERT measured precipitate weight still makes no obvious influence on the aforementioned trend.

The carbon concentration in the matrix was calculated by subtracting the carbon concentration in carbides from the nominal chemical composition. Fig. 6 shows the calculated carbon concentration in the matrix (denoted as open squares) as a function of *TP*. The error bar of each data indicates the standard deviation. The solid line is provided to guide the eye and the dot-and-dash line denotes the nominal chemical composition of carbon in F82H steel. One can note that the carbon concentration was 0.09 wt.% at *TP* below 15.3, then it sharply dropped down to nearly zero at the *TP* range from 15.3 to 16.2. As per the Thermo-Calc calculation, the carbon concentration in the matrix of well-tempered F82H was extremely low, which is roughly consistent with the solid solubility of carbon in α phase of Fe-8Cr system, i.e.: 0.0035 wt.%. On account of the fact that the carbon concentration in the matrix is estimated close to zero, it is inferred that the nominal crystal structure of tempered F82H steel is bcc, rather than bct. Here, the uncertainty of the measured carbon concentration should be noticed, which mainly stems from the following factors: (a) not high enough resolution on carbon concentration of ERT method, and (b) not accurate enough carbon concentration in this material. This is also the reason why the estimated carbon concentration was even slightly lower than zero and a quite large error bar was present.

3.3. Estimation of precipitation strengthening in F82H specimen

Thus far, it is believed that F82H steels exhibit excellent mechanical properties, mainly profiting from the lath martensitic structure and the fine particles embedded in the matrix. Since the quantitative characterizations of carbides in tempered F82H steel is successfully attained in this study, a quantitative estimation of the precipitation strengthening at room temperature can be performed.

The tensile strength contributed from precipitation strengthening (σ_{PPT}) is generally interpreted by Orowan [25] and/or Ashby-Orowan strengthening mechanism [26], the strength increase by Orowan (σ_O) and Ashby-Orowan ($\sigma_{A\text{-}O}$) mechanism is given by Eqs. (6) and (7), respectively:

$$\sigma_O = \frac{0.8MGb}{L} \tag{6}$$

$$\sigma_{A-O} = \frac{0.8MGb}{2\pi\sqrt{1-\nu}L} \cdot \ln\left(\frac{x}{2b}\right) \tag{7}$$

where M, G, b, ν, L and x are Taylor factor (=3.06 for random textured bcc metals [27]), shear modulus (=81.6 GPa [28]), burgers vector (=0.248 nm), Poisson's ratio (=0.293 in bcc iron [28]), average inter-particle spacing and average particle diameter on the slip planes, respectively. Also, L and x are given by the following equations, assuming that particles are randomly distributed in the matrix:

$$L = \sqrt{\frac{2}{3}}\left(\sqrt{\frac{\pi}{f}} - 2\right)r \tag{8}$$

$$x = 2\sqrt{\frac{2}{3}} \cdot r \tag{9}$$

where f and r are volume fraction and particle size of carbides, respectively. The value of σ_O is derived assuming that the energy of dislocation per length is approximated to be $Gb^2/2$, while the

$\sigma_{A\text{-}O}$ is derived by taking the energy of bowed-out edge or screw dislocations around the carbide into consideration.

The proof strength ($\sigma_{0.2}$) of tempered F82H at room temperature was 525 ± 25 MPa [29]. Assuming a random dispersion of the carbides, the calculated σ_O was 8.0 and 44.1 MPa for MX and $M_{23}C_6$, respectively. The total precipitation strength from both MX and $M_{23}C_6$ ($\sigma_{PPT} = \sigma_{PPT,MX} + \sigma_{PPT,M23C6}$) was 52.1 MPa. The ratio between precipitation strength and overall proof strength ($\sigma_{PPT}/\sigma_{0.2}$) was approximately 9.9% in the case of Orowan mechanism. On the other hand, the values of the calculated $\sigma_{A\text{-}O}$ were 3.8 and 21.8 MPa for MX and $M_{23}C_6$, respectively. The $\sigma_{PPT}/\sigma_{0.2}$ ratio was 4.9% in the case of Ashby-Orowan mechanism. Kamikawa et.al. [30] reported that the Orowan mechanism is predisposed to overestimated the precipitation strengthening from nanometer-scale particles while the Ashby-Orowan mechanism can reasonably explain the strengthening at least in the average particle diameter range of 3–20 nm. Taking the microstructure into consideration, where $M_{23}C_6$ particles of 55 nm average size are preferably located along the grain boundary as shown in Fig. 3(a), the precise estimation may not be able to be deviated from Ashby-Orowan model; The frequency to pin the dislocation motion by grain boundary particle is lower than the intragranular one. However, in any case, the actual strength increment by precipitates is lower than that assumed from Orowan model. Therefore, the actual precipitation strengthening is presumed to lie between $\sigma_{A\text{-}O}$ and σ_O: i.e. $4.9\% < \sigma_{PPT}/\sigma_{0.2} < 9.9\%$. It obviously demonstrates that the fine particles in F82H steel do not greatly improve the tensile strength at room temperature. Nevertheless, the presence of these precipitates is believed to play a significant role on the materials' other mechanical performance. For example, Tamura et.al. [9] reported the effect of tantalum on creep properties. The creep strength surely increased by $\approx 17\%$ within the range of 0.04 wt.% in tantalum concentration in F82H steel. Thus, they carbides play an indispensable role as obstacles to impede the dislocation motion, when it comes to dislocation movement happening during creep deformation and thermal aging.

4. Conclusions

The precipitation in F82H steels and Fe-0.2TaC model alloy were investigated by both TEM observation and extracted residue tests. The precipitation strengthening and its effect on tensile strength at room temperature was quantitatively estimated based on the Orowan and the Ashby-Orowan mechanism. In summary, the following results were obtained.

(1) TEM observation and extracted residue test combined with XRD analysis were conducted to characterize the carbide in Fe-0.2TaC and tempered F82H. The ratio between the total volume of carbide evaluated by TEM and extracted residue test in Fe-0.2TaC was estimated approximately as1.84; in contrary, this ratio was 0.54 for tempered F82H steel. This inconsistency is considered to originate from the microstructural features, such as particle size and shape.
(2) Effects of tempering on the precipitation in F82H steels were further investigated by extracted residue tests, combined with XRD analysis. It was found that the amount of carbides rapidly increased in the *TP* range from 15.3 to 16.2.
(3) Tensile strength increment contributed by carbides in F82H steel, σ_{PPT}, was estimated based on the Orowan and the Ashby-Orowan mechanism. The σ_{PPT} in F82H steel was between $4.9 \sim 9.9\%$ of its overall $\sigma_{0.2}$, demonstrating that the carbides in F82H steel are less effective to improve the tensile strength at room temperature, although its advantageous effect on creep strength has been clarified previously.

Acknowledgment

This study has been prepared as an account of work assigned to the Japanese Implementing Agency under the Procurement Number IFERC-T3PA03-JA within the "Broader Approach Agreement" between the Government of Japan and the European Atomic Energy Community and under the auspices of the JWRI Collaboration Research program. A part of this work is supported by a project "R&D of nuclear fuel cladding materials and their environmental degradations for the development of safety standards" entrusted to Tohoku University by Ministry of Education, Culture, Sport, Science and Technology of Japan.

References

[1] A. Alamo, J.C. Brachet, A. Castaing, C. Lepoittevin, F. Barcelo, Physical metallurgy and mechanical behaviour of FeCrWTaV low activation martensitic steels: effects of chemical composition, J. Nucl. Mater. 258–263 (1998) 1228–1235.
[2] A. Hishinuma, A. Kohyama, R.L. Klueh, D.S. Gelles, W. Dietz, K. Ehrlich, Current status and futher R&D for reduced-activation ferritic/martensitic steels, JNM 258-263 (1998) 193–204.
[3] X. Jia, Y. Dai, Microstructure and mechanical properties of F82H weld metal irradiated in SINQ target-3, J. Nucl. Mater. 329-333 (2004) 309–313.
[4] X. Jia, Y. Dai, Micro-hardness measurement and micro-structure characterization of T91 weld metal irradiated in SINQ target-3, J. Nucl. Mater. 343 (2005) 212–218.
[5] H. Tanigawa1, A. Sawahata, M.A. Sokolov, M. Enomoto, R.L. Klueh, A. Kohyama, Effects of inclusions on fracture toughness of reduced-activation ferritic/martensitic F82H-IEA steels, Mater. Trans. 48 (2007) 570–573.
[6] T. Nagasaka, Y. Hishinuma, T. Muroga, Y. Li, H. Watanabe, H. Tanigawa, H. Sakasegawa, M. Ando, Extraction residue analysis on F82H-BA07 heat and other reduced activation ferritic/martensitic steels, Fusion Eng. Design 86 (2011) 2581–2584.
[7] H. Sakasegawa, H. Tanigawa, S. Kano, M. Enomoto, Precipitation behavior in F82H during heat treatments of blanket fabrication, Fusion Eng. Design 86 (2011) 2541–2544.
[8] F. Abe, S. Nakazawa, H. Araki, T. Noda, The role of microstructural instability on creep behaviour of a low radioactivation martensitic 9Cr-2 W steel, Metal. Trans. A 23 (1992) 469–477.
[9] M. Tamura, H. Hayakawa, M. Tanimura, A. Hishinuma, T. Kando, Development of potential low activation ferritic and austenitic steels, J. Nucl. Mater. 141-143 (1986) 1067–1073.
[10] M. Tamura, K. Ikeda, H. Esaka, K. Shinozuka, Precipitation behavior of NbC in 9%Cr1%Mo0.2%VNb steel, ISIJ Int. 41 (2001) 908–914.
[11] Fumio Kurosawa, Masao Saeki, Future aspects of state analysis of ferrous materials, Tetsu-to-Hagane 76 (1990) 483–494 (in Japanese).
[12] M. Tamura, H. Kusuyama, K. Shinozuka, H. Esaka, Tempering process and precipitation behavior of 8%Cr–2%WTa steel, ISIJ Int. 47 (2007) 317–326.
[13] H. Li, D. Mitchell, Microstructure characterization of P91 steel in the virgin, service exposed and post-service re-normalized conditions, Steel Res. Int. 84 (2013) 1302–1308.
[14] H. Abe, T. Ishizaki, F. Li, S. Kano, Y. Li, Y. Satoh, T. Nagase, H. Yasuda, New approach to in situ observation experiments under irradiation in high voltage electron microscopes, Mater Trans 55 (2014) 423–427.
[15] F. Tavassoli, Fusion Demo Interim Structural Design Criteria (DISDC) / Appendix A: Material Design Limit Data / A3.S18E Eurofer Steel, Appendix A (2004) pp. 15.
[16] K.S. Edmund, The Refractory Carbides, vol. 2, Academic Press, Inc., 1967.
[17] M. Tamura, H. Sakasegawa, K. Shiba, H. Tanigawa, K. Shinozuka, H. Esaka, Decomposition of Y2Ti2O7 particles in 8 Pct Cr oxide-dispersion-strengthened martensitic steel during tempering, Metall. Mater. Trans. A 42 (2011) 2176–2188.
[18] International Centre for Diffraction Data, Public Report 2002, (2002) 4–5.
[19] I. Nitta, The X-Ray Crystallography, MARUZEN Publishing Co., Ltd, 1959 (In Japanese).
[20] B.D. Cullity, Elements of X-Ray Diffraction, 2nd edition, Addison Wesley Publishing Co. Inc., 1978.
[21] LINUS PAULING FILE Multinaries Edition – 2012, SpringerMaterials Release 2014, sd 0526282.
[22] J.H. Hollomon, J.D. Jaffe, Time–temperature relations in tempering steel, Trans. AIME 162 (1945) 223–249.
[23] V. Dudko, A. Belyakov, R. Kaibyshev, Effect of tempering on mechanical properties and microstructure of a 9% Cr heat resistant steel Mater. Sci. Forum, 706-709 (2011) 841–846.
[24] W.F. Hosford, Iron and Steel, Cambridge University Press, 2012.
[25] E. Orowan, in: Symposium on Internal Stresses. Metals and Alloys, London, 1948, p. 451.
[26] T. Gladman, D. Dulieu, I. McIvor, Structure-property relationships in high--strength microalloyed steels, in: Micro Alloying 75 Proceedings, New York, 1997, pp. 32–52.

Please cite this article as: S. Kano et al., Precipitation of carbides in F82H steels and its impact on mechanical strength, Nuclear Materials and Energy (2016), http://dx.doi.org/10.1016/j.nme.2016.09.017

[27] N. Hashimoto, T.S. Byun, K. Farrel, S.J. Zinkle, J. Nucl. Mater. 336 (2005) 225–232.
[28] G.W.C. Kaye, T.H. Laby, in: Tables of Physical and Chemical Constants, 14th edn., Longman, London, 1973, p. 31.
[29] T. Hirose, H. Sakasegawa, M. Nakjima, H. Tanigawa, Mechanical properties of TIG and EB weld joints of F82H, Fusion Eng. Design (2015) (In press).
[30] Naoya Kamikawa, Kensuke Sato, Goro Miyamoto, Mitsuhiro Murayama, Nobuaki Sekido, Kaneaki Tsuzakie, Tadashi Furuhara, Stress–strain behavior of ferrite and bainite with nano-precipitation in low carbon steels, Acta Mater. 83 (2015) 383–396.

Please cite this article as: S. Kano et al., Precipitation of carbides in F82H steels and its impact on mechanical strength, Nuclear Materials and Energy (2016), http://dx.doi.org/10.1016/j.nme.2016.09.017